Arabian Journal of Chemistry (2020) 13, 6662–6671

King Saud University

Arabian Journal of Chemistry

www.ksu.edu.sa
www.sciencedirect.com

ORIGINAL ARTICLE

Two Cu(II) coordination polymers: Photocatalytic Cr(VI) reduction and treatment activity on influenza A virus infection by inducing IFN-γ expression

Liang Chen [a,*], Jun Chen [b], Li-Mei Zhu [c]

[a] Department of Infectious Disease, Beijing Jishuitan Hospital, 4th Medical College of Peking University, Beijing, China
[b] Department of Pathology, Nanjing Drum Tower Hospital, the Affiliated Hospital of Nanjing University Medical School, Nanjing, China
[c] Department of Chronic Disease and Infectious Disease Control, Jiangsu Provincial Center for Disease Control and Prevention, Nanjing, China

Received 7 May 2020; revised 18 June 2020; accepted 18 June 2020
Available online 25 June 2020

KEYWORDS

Coordination polymer;
Photocatalytic Cr(VI) reduction;
Influenza A virus infection;
GTU

Abstract With H_4L (5,5′-(1,3,6,8-tetraoxobenzo [lmn] [3], [8] phenanthroline-2–7-diyl) bis-1,3-benzenedicarboxylic acid), the rigid π-conjugated connector reacting with different N-donor auxiliary connectors and $Cu(NO_3)_2{\cdot}3H_2O$ under the solvothermal conditions, two new coordination polymers (CPs) based on Cu ions as nodes $\{[Cu(H_2L)(4,4'\text{-bibp})(H_2O)_2]\}_n$ (**1**) and $\{[Cu(L)_{0.5}(4,4'\text{-bimb})(H_2O)_2]{\cdot}3{\cdot}.5H_2O{\cdot}2DMA\}_n$ (**2**) {4,4′-bimb = 4,4′-bis(imidazol-1-ylmethyl) bipheny and 4,4′-bibp = 4,4′-bis(imidazolyl)biphenyl, DMA = N,N- dimethylacetamide} were prepared and characterized. The photocatalytic reduction of Cr(VI) and dye degradation were performed with these two CPs. The results showed that under the ultraviolet irradiation, they revealed excellent photocatalytic reduction of Cr(VI) in thirty minutes, and the reduction efficiency was over 98%. According to results of the *in vitro* macrophage infectious model, in comparison with complex **2,** complex **1** has stronger treatment activity on influenza A virus infection. Then, the ELISA test exhibited that complex could significantly regulated the releasing the INF-γ, but not complex **2**.

* Corresponding author.
E-mail address: c_liang01@126.com (L. Chen).
Peer review under responsibility of King Saud University.

Production and hosting by Elsevier

https://doi.org/10.1016/j.arabjc.2020.06.021

Next, the results of RT-PCR suggested that complex **1** is much better than complex **2** on reducing the relative expression of the interferon inducible transmembrane proteins (IFITM). Finally, the western blot further confirmed the induced ability of complex **1** on the IFITM in protein level.

1. Introduction

Influenza A virus is one of the viruses that serious threat human's health. Traditional antiviral drugs are mainly targeted at viral proteins, aimed to reduce the virus replication (Yanagi and Ozawa, 2019). However, due to the rapid mutation of viruses, many traditional drugs are difficult to exert their expected effects as we expected. Studies have found that hundreds of cytokines are involved in the process of virus infection of immune cells, suggesting that we should the change the strategy about anti-virus treatment from targeting viral proteins to affecting host cytokines, and then exert the excellent anti-virus activities (Bailey, 2020; Mifsud et al., 2020; Chao et al., 2020).

In recent decades, coordination polymer (CPs) or metal-organic frameworks (MOFs) consisted of the bridging organic ligands and metal clusters/ions through the interaction of coordination bond have gained great attentions (Li et al., 2019; Xu et al., 2018; Tang et al., 2016). CPs have the advantages of the coordination complexes and the semiconductor materials, which could be applied in many important domains such as heterogeneous catalysis and biomedicine simultaneously (Zhang et al., 2016, 2019; Chen et al., 2019; Pan et al., 2018; Feng et al., 2017). Since the first report of MOF-5 as the semiconductor material, many MOF-based materials have been applied as the photocatalytic materials for the degradation of organic dyes and reduction of Cr(VI) ions in water, and many of them are u depending on the ligands used (Feng et al., 2013; Duan et al., 2 2020b). So the selection of suitable organic ligands plays a key in the final properties of the targeted CPs. Naphthalenediimi (NDI) derivatives are versatile in coordination and hemistry due to their large conjugated planar structure spec electron transfer properties. Its coordination complexe w prop g appli-cations in such fields as DNA intercalators, lu sc photocatalysis (Chen and Zhang, 2019; khopa et al., 2006; Stewart, 1981). On the other hand, m Cu(II)-cont coordination complexes were found to show iferative, cyt antitumour and genotoxic activities (B -Gó al., 2009; Ruiz-Azuara and Bravo-Gomez, 2010; Ri -Müller et a 07; Cui et al., 2019). Another drive for targeti pper(II) was due less toxic nature, which can be further d sed on mplexation w ligands and thus proved promising i deve ment of copper complexes as the bioactive reagents. In rch, two w Cu-based coordination polymers (CPs {[Cu(I 4,4′-bi $H_2O)_2]\}_n$ (**1**) and $\{[Cu(L)_{0.5}$ (4,4′-bimb)(H_2O2D {4,4′-bimb = 4,4′-bis(imidazol-1-ylmeth biphen nd 4,4′- = 4,4′-bis(imidazolyl)biphenyl} were p ed b naphthalenediimide-type ligand H_4L (5,5′-(1,3,6,8-t ize], [8] phenanthroline-2–7-diyl) bis-1,3-benzenedica lic acid) and characterized via the analysis of single-crystal X diffraction, elemental analysis and infrared spectroscopy (IR). Th otocatalytic reduction of Cr(VI) and dye degradation were performed with these two CPs. The results showed that under the ultraviolet irradiation, they revealed excellent photocatalytic reduction of the Cr(VI) in thirty minutes, and the efficiency of reduction was over 98%. The treatment activity of two complexes was assessed and the specific mechanism was also discussed. The treatment activity of the complexes on influenza A virus infection was measured with viral gene transduction (GTU). Then, the ELISA was conducted to detect the cytokines levels after complexes treatment. In addition to this, the relative of the interferon inducible transmembrane proteins (IFITM) was determined by the real time RT-PCR. Finally, the expression of IFITM in protein level was detected with Western blot assay.

2. Experimental

2.1. Chemicals and measurements

All the organic ligands u in thi udy w btained from Shanghai Chemsoon C ical T nology Co., Ltd (Shanghai, China) and us s r . Other vents and reagents utilized in this arch co e b ght from commercial sources and t uld be utili h no purification. Carbon, nitrog and ogen were analyzed with the elemental analytical instrument ario MACRO cube. The IR spectre betw 0 and 400 c were carried out using the FTIR–84 Spectrometer using the KBr pellets. Ultraviolet–visible D for the sol amples were determined via the spectrophoto er of Perk Elmer Lambda 650S, with the $BaSO_4$ as stan possess 100% reflection. The reduction amount of Cr(VI) alyzed on a Varian ultraviolet–visible-light V–vis) spectrophotometer (Cary − 50, Varian Co.) and d colorimetrically at 540 nm using the diphenylarbazide method. The reduction ratio of Cr(VI) is calculated using the following expression: Reduction ratio of Cr(VI) = $(C_0 - C_t)/C_0 \times 100\%$, Where C_0 and C_t are the absorbance intensities of illuminated for 0 and t min, respectively.

3. Preparation and characterization for $\{[Cu(H_2L)(4,4'\text{-bibp})(H_2O)_2]\}_n$ (1) and $\{[Cu(L)_{0.5}(4,4'\text{-bimb})(H_2O)_2]\cdot 3.5H_2O\cdot 2DMA\}_n$ (2)

For complex **1**, a mixture of H_4L (0.016 mmol, 9.50 mg) $Cu(NO_3)_2\cdot 3H_2O$ (0.01 mmol, 24 mg), 4,4′-bibp (0.016 mmol, 4.58 mg), DMA (2.0 mL) as well as H_2O (2 mL) was stirred in a beaker for 30 min, then the mixture was sealed in a 25 mL of stainless steel container lined with the Teflon and heated for three days at 120 °C. After cooling to room temperature, green crystals of the complex **1** were obtained with a yield of 39% (on the basis of H_4L). Calcd (%) for $C_{48}H_{30}N_6CuO_{14}$: C, 59.20; H, 3.08; N, 8.63, found: C, 59.22; H, 3.30; N, 8.34. IR data (cm^{-1}): 3444(s), 3103(s), 2360(vs), 2339(m), 1710 (w) 1610(s), 1562(m), 1527(m), 1460(w), 1380(s), 1134(vs), 1072 (s), 962(s), 933(s), 837(s), 775(vs), 649(s).

For complex **2**, a mixture of $Cu(NO_3)_2\cdot 3H_2O$ (0.01 mmol, 24 mg), H_4L (0.004 mmol, 2.38 mg), 4,4′-bimb (0.004, 1.26 mg), 0.5 mL of N, *N*-dimethyl acetamide (DMA) as well as 0.5 mL H_2O was stirred in a beaker for 30 min, then the mixture was transferred into the rigid glass tube, sealed and heated for three days at 120 °C. After cooling glass tube to the room temperature, dark blue crystals of complex **2** was

obtained with a yield of 33% (on the basis of H_4L). Analysis calcd (%) for $C_{62}H_{66}N_{12}Cu_2O_{23}$: C, 50.82; H, 4.37; N, 11.48. Found: C, 50.23; H, 4.03; N, 11.28. IR data (cm^{-1}): 3442 (s), 2362 (m), 1679 (m), 1650 (m), 1612 (s), 1558 (vs), 1521 (m), 1402 (m), 1346 (w), 1251 (s), 1091 (s), 1027 (w), 945 (m), 746 (w), 717 (m),651 (s).

With the diffractometer of Oxford XcaliburE we obtained the data of X-ray. The software of crysalispro was applied to analyze the strength data and convert the strength data into the HKL files. The program of SHELXS inaccordance with direct method was utilized to build the initial framework model for the complex **1**, and the program of SHELXL-2014 inaccordance with least square means was modified. Mixing anisotropic parameters with **1**'s non-H atoms. Then all of the hydrogen atom via applying the AFIX command to geometrically fix on the C atom they are bridged to. For the highly disordered nature of the lattice DMA molecules, some of them could not be well modeled in the refinement. Final refinement was performed with modification of the structure factors for contribution of the disordered solvent electron densities using the *SQUEEZE* option of *PLATON*. The final chemical formula of 2 was determined via a combination of the results from the single crystal X-ray diffraction along with the elemental analysis. Table 1 details the crystallographic parameters as well as the refinement of these two complexes.

3.1. Photocatalytic tests

The photocatalytic experiments for Cr(VI) reduction [illegible] $K_2Cr_2O_7$ aqueous solution were conducted at ambient [illegible]

Table 1 Refinement details and crystallo[illegible]phic [illegible]ameters for complexes **1** and **2**.

Identification code	**1**	
Empirical formula	$C_{48}H_{30}Cu$[illegible]$_{14}$	C_{82}[illegible]$Cu_2N_{13}O_{26}$
Formula weight	978.32	1805.7
Temperature/K	293.1	293.15
Crystal system	tri[illegible]inic	monoclinic
Space group	[illegible]	$P2_1/c$
a/Å	6.9913(4)	14.4269(11)
b/Å	8.36[illegible])	22.021(5)
c/Å	[illegible]980(10)	16.6247(8)
α/°	[illegible]69(4)	90
β/°	9[illegible]	98.9660(10)
γ/°	89.0[illegible]0)	90
V[illegible]e/Å^3	945.28(4)	5217.1(13)
Z	[illegible]	2
ρ_{calc}g/c[illegible]	1.719	1.150
μ/mm^{-1}	0.669	0.478
Data/restraints/parameters	4121/2/320	11884/171/593
Goodness-of-fit on F^2	1.056	0.991
Final R indexes [$I \geq 2\sigma$ (I)]	R_1 = 0.0393, ωR_2 = 0.1046	R_1 = 0.0726, wR_2 = 0.1969
Final R indexes [all data]	R_1 = 0.0540, ωR_2 = 0.1145	R_1 = 0.1262, wR_2 = 0.2298
Largest diff. peak/hole/e Å^{-3}	0.30/−0.55	0.98/−0.63
CCDC	1,990,495	1,990,496

tions in a quartz reactor containing 15.0 mg photocatalyst and 200 mL of 10 mg·L^{-1} Cr(VI) solution. After stirring for 30 min to reach adsorption-desorption equilibrium, the suspensions were irradiated by a 500-W Hg lamp (Beijing Aulight Co., Ltd). During the photocatalytic degradation experiments, 1.5 mL aliquots were extracted at 3 min intervals for analysis. The Cr(VI) content in the supernatant was determined colorimetrically at 540 nm using the diphenylcarbazide (DPC) method. Additionally, two cationic organic dyes, MB (10 mg·L^{-1}) and RhB (10 mg·L^{-1}), and two anionic organic dyes, MO (10 mg·L^{-1}) and X-3B (50 mg·L^{-1}), were selected as organic pollutant models to evaluate [illegible]otocatalytic performances of **1** under the same co[illegible]ions. [illegible]spec Alpha-1860 spectrometer was used t[illegible]onitor the [illegible]centration changes determined at the maximu[illegible]bsorbance[illegible] 664, 554, 463 and 540 nm for MB, [illegible], MO a[illegible]X-3B, [illegible]pectively.

3.2. GTU determinati[illegible]

After synthesi[illegible] comple[illegible]1 and [illegible]their inhibition against the influenz[illegible]irus invasio[illegible]ty into macrophages was evaluated[illegible]his [illegible]formation w[illegible]s carried out under instructions' guidance wit[illegible]ght modifications. In short, the macroph[illegible]the phage o[illegible]ical growth were harvested in the cell c[illegible]ure plates, then the influenza A virus were added into cells [illegible]the ratio of [illegible]:1. Next, complex **1** or **2** was added for treat[illegible]t. After t[illegible] the virus in the cells were isolated and the n[illegible]ers of [illegible] influenza A virus in the cells were detected by [illegible] the viral gene transduction of influenza A.

[illegible]ELISA detection

The inflammatory cytokines from the influenza A infected macrophages was evaluated by the ELISA test kit. This experiment was performed on the basis of the protocols with slight modification. In short, the macrophages in the phage of logical growth were harvested in the cell culture plates, then the influenza A virus were added into cells at the ratio of 10:1. Next, the complex **1** or **2** was added to perform the treatment at 5, 10, 50 μg/mL concentration. After treated for one day, the cell supernatant was collected and the content of the INF-γ released from macrophages was detected via the ELISA method. This preformation was carried out for three or more times.

3.4. Real time RT-PCR

The real time RT-PCR was performed in this research to assess the influence for the complex **1** or complex **2** against the *ifitm* gene expression in infected macrophages. This preformation was carried out in accordance with instructions. As described above, the macrophages were infected with influenza A virus and then treated with complex **1** or **2**, we extracted overall RNA in infected macrophages by the TRIzol Reagent in accordance with the instructions of manufacturer. And then, the quality as well as quantity of the extracted RNA was determined by the instrument of NanoDrop 2000C. And we reverse transcripted overall RNA into the cDNA by the Reverse Transcription Kit, then the SYBR Green Master Mix (Roche) was carried out for the *ifitm* gene expression detection in infected macrophages, in which the *gapdh* gene was utilized as internal

control. All of data were determined via utilizing the $2^{-\Delta\Delta Ct}$ approach as the comparative quantification.

3.5. Western blot

The expression of the IFITM on infected macrophages was further confirmed with western blot. This experiment was finished in accordance with the instructions of manufacturer. In short, the macrophages were infected with influenza A virus and then treated with complex **1** or **2**. The macrophages were lysed with lysis buffer, and total protein was harvested. Then the BCA Protein Assay kit (23225, Pierce, USA) was used for the detection of the concentrations of protein samples. Next, we loaded the protein samples on 10% modified gels of sodium dodecyl sulfate-polyacrylamide and then transferred them onto the membrane of polyvinylidene difluoride (PVDF). After sealing in skim milk of 5%, the membranes were seeded by the suitable primary antibody against IFITM or GAPDH overnight at 4 °C. After incubation for 60 min with the horseradish peroxidase-conjugated secondary antibody, proteins were visualized utilizing an increased chemiluminescence (ECL) detection kit (Thermo Fisher Scientific) and quantified using ImageJ software (BIO RAD).

4. Results and discussion

4.1. Structure description of 1 and 2

The as-prepared H_4L ligand has little solubility in M… CH_3CN and EtOH and other familiar organic solvents … could be dissolved in DMA. So the targeted complex **1** w… prepared using DMA as the main solvent. On the basis of the crystal data harvested under the room temperature, the results for the structural solution as well as the refinement indicated that the complex **1** is part of triclinic system with space group P-1 and revealed a two-dimensional layered network. As exhibited in the Fig. 1a, its asymmetric unit is consisted of an absolute Cu^{2+} ion, 0.5 ligands L^{4-}, 0.5 4,4′-bibp as well as a coordinated molecule of H_2O. The Cu^{2+} ion is 6-coordinated via two carboxylate oxygen-atoms of O1i and O1 of two connectors L^{4-}, two N atoms of N2i and N2 in two 4,4′-bibp as well as two oxygen-atoms of O1Wi and O1W in two coordinated water, reflecti… …htly distorted geometry of octahedron $\{CuN_2O_4\}$. T… …engths … …Cu-O bond are 2.0853(15) Å and 2.0632(12) … …nd the leng… …of Cu-N bond is 2.0653(16) Å. Particularly, … …symmetri… …nds for the Cu(II) ions are combine… … the id… …al at… … at 180° bond angles (N2-Cu1-N2… …O1W-Cu1-O… …d O1-Cu1-O1i, symmetry code i: … …-y, 2-… …ome dep… …ons of ligands H_4L are carried out an… …ared sp…tra also confirmed that the bending … …ation … …ell as … …tching vibration for the group –O… … carboxylic … …up of complex **1** was respectively … …sc… … at 933 c… … and 3444 cm^{-1}. The H_2L^{2-} anions use t… …onodentate coordination pattern to link th… $^{2+}$ ions ge… …ting a one-dimensional wave-like $[Cu…L]_n$ chain (Fig. 1b). Meanwhile, the ligands 4,4′-bibp br… …e to the neighbouring Cu^{2+} ions in order to generate a… …er one-di… …sional $[Cu(4,4'\text{-bibp})]_n$ chain with wave sha… Ultimate… …both the two one-dimensional chains intersect … …ther to acquire a two-dimensional layer network on plane ac (Fig. 1c), which is deep expanded into the … …dimensional supramolecular skeletons through the intermolecular hydrogen-bonding (Fig. 1d). Topologically, when

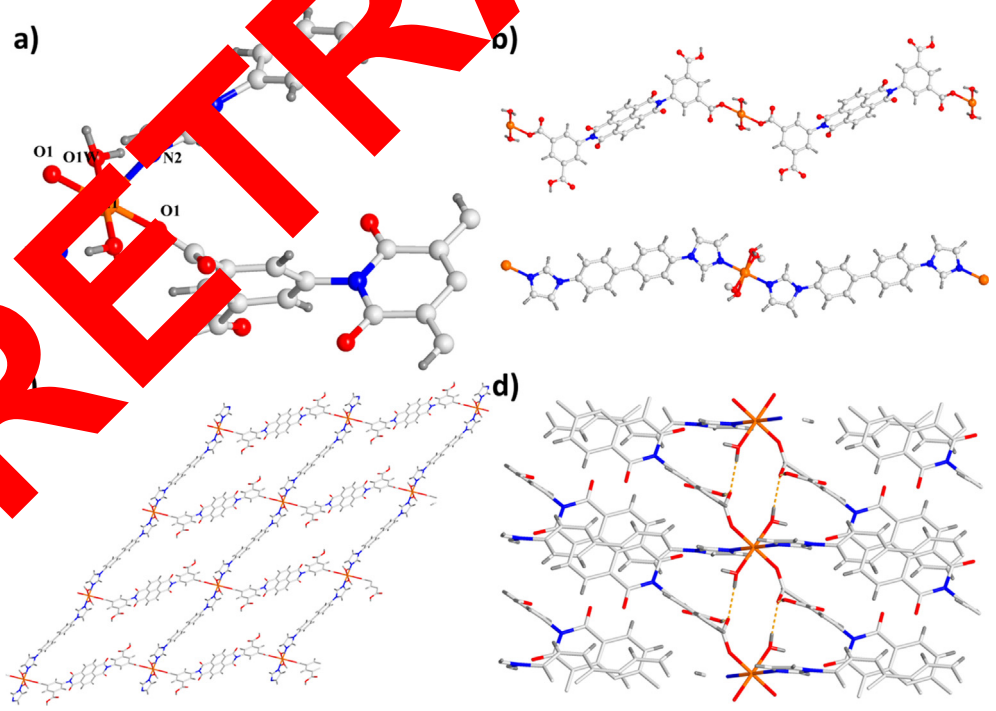

Fig. 1 (a) The asymmetric unit view for the complex **1**. (b) The one-dimensional framework with chain-shape for the complex **1**. (c) two-dimensional layered network for the the complex **1**. (d) three-dimensional supramolecular skeleton generated via the interactions of H-bond.

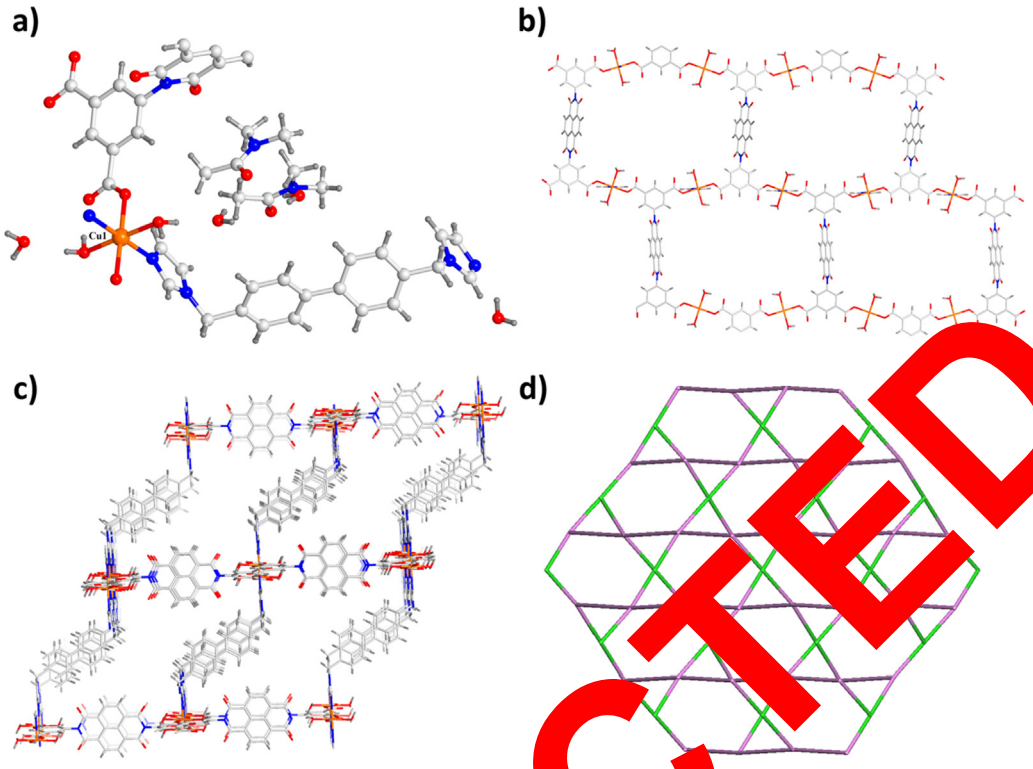

Fig. 2 (a) The asymmetric unit view for the complex **2**. (b) The two-dimensional layered network for the complex **2**. (c) The three-dimensional pillar-layered network for the complex **2**. (d) The four-linked skeleton view for the complex **2**.

the ligands 4,4′-bibp and H_2L^{2-} can be regarded as two-linked nodes, complex **2** reflects a four-nodal net with 7271 Å² 21.8052 Å quadrilateral size and $\{4^4.6^2\}$ symbol.

Complex **2** was generated utilizing the condition of reaction similar to that of complex **1** except the substitution of 4,4′-bibp ligand by 4,4′-bimb ligand. In the basis of the crystal data which harvested under the room temperature, the results for the structural solution as well as the refinement indicated that complex **2** was crystalized in monoclinic system space group P21/c and presents a three-dimensional pillar-layered network. Its asymmetric unit is composed of a Cu^{2+} ion, 0.5 L^{4-} connectors, 4,4′-bimb, two coordinated H_2O, 3.5 lattice H_2O as well as two DMA (Fig. 2a). Each Cu1 ion is 6-coordinated through six distinct carboxylic acid oxygen-atoms, the length of Cu1-O1 is 2.082(2) Å, and the length of Cu1-O4ii is 2.071(2) Å, symmetry code ii: 1 − *x*, −1/2 + *y*, 1 − *z*. Two oxygen-atoms in the molecules of water (with the Cu1-O1W length of 2.102(2) Å, and the Cu1-O2W length of 2.104(2) Å), and two nitrogen-atoms in two ligands 4,4′-bimb (with the Cu1-N2 length of 2.062(3) Å, and Cu1-N5i length of 2.063(3) Å), generating a geometry of pseudo-octahedron. The H_4L connectors in complex **2** are fully deprotonized, and without strong bands were respectively discovered from 2500 to 3400 cm^{-1} and between 900 and 950 cm^{-1}. In complex **2**, the ligands H_4L also utilize single tooth coordination pattern to link with the Cu^{2+} ions generating the two-dimensional layer $[Cu_2L]_n$, it looks like a window of rectangle, about 13.106(11) × 21.916(2) Å² (Fig. 2b). One dimensional V-shaped chains generated via the ligands 4,4′-bimb in adjacent layers is strung into three-dimensional structure (Fig. 2c). In topology, each ligand L^{4-} is viewed as a four-linked node, so the three-dimensional skeleton can be simplified as the four-linked net, and the symbol is $\{6^4.8^2\}$ (Fig. 2d).

To check the phase purity of the products, powder X-ray diffraction (PXRD) experiments have been carried out for these complexes (Fig. S1, Supporting Information). The peak positions of the experimental and simulated PXRD patterns are in good agreement with each other, indicating that the crystal structures are truly representative of the bulk crystal products. The differences in intensity may be owing to the preferred orientation of the crystal samples. To investigate the stabilities of complexes **1** and **2**, TG analysis was carried out in the temperature range of 25 to 800 °C under the N_2 atmosphere. As displayed in Fig. S2, complex **1** shows a slight weight loss of 3.52% from 100 to 340 °C, which is ascribed to the release of two coordinated water molecule (calcd 3.70%). After the temperature of 350 °C, a sharp weight loss could be observed, indicating the decomposition of the organic ligand as well as the collapse of the whole framework. For complex **2**, the curve shows a significant decrease of 29.32% from 25 °C to 270 °C, which corresponds to the release of two coordinated water, three and a half lattice water and two lattice DMA molecules (calcd 29.01%).

4.2. Catalytic Cr(VI) reduction

The optical performances of complexes **1** and **2** were determined via the ultraviolet–visible DRS. According to Fig. 3a and b, the bands of absorption were respectively at 390 as well as 490 nm. The values of band gap (Eg) were evaluated

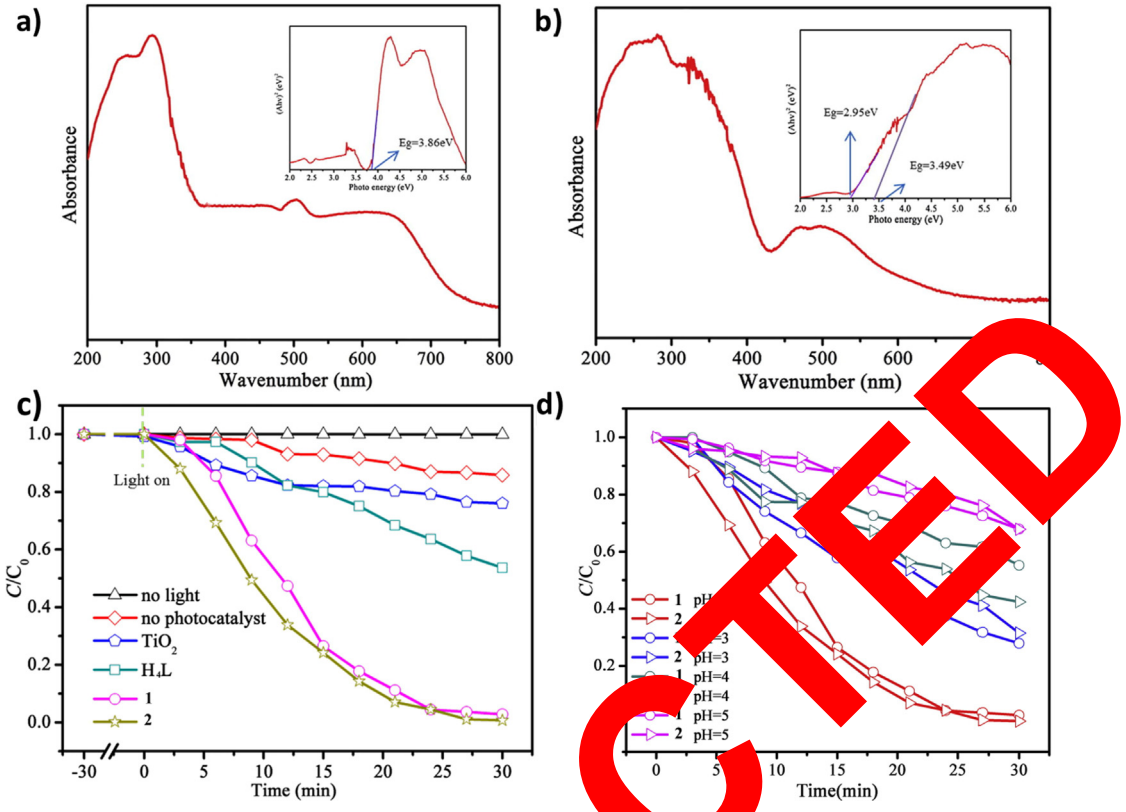

Fig. 3 Ultraviolet–visible spectra of complexes **1** (a) and **2** (b). (c) Photocatalytic reduction of Cr(VI) rates of distinct photocatalysts under the same condition. (d) Photocatalytic reduction of Cr(VI) with complexes **1** and **2** as the photocatalysts under ultraviolet irradiation at distinct pH values.

utilizing the $(Ahv)^2$ versus hv, in which v, h a[illegible] light frequency, the Planck constant as well as [illegible]rbance [illegible]nstant, respectively. And the values of Eg can be [illegible]ate for complex **2** and 3.86 eV for com[illegible] **1**, su[illegible]ng that the two kinds of MOFs are the late[illegible]hotocataly[illegible]ontaining wide band gap. The reduction [illegible]ies of Cr(V[illegible]r complexes **1** and **2,** P25 (the comm[illegible]cial [illegible]lity for the titanium dioxide), free H_4L, und[illegible]he irradiati[illegible]f ultraviolet are revealed in the Fig. 3[illegible]bout 99% and 9[illegible] for the Cr(VI) were decreased into[illegible](III) [illegible] the irradiation of ultraviolet after half an hour w[illegible]ex **2** and complex **1** as the photocatalysts in w[illegible], resp[illegible]ely. Wh[illegible], in the existence of P25 and the fr[illegible]s the [illegible]talysts, only 46% and 24% of the C[illegible]I) red[illegible]tion rate[illegible]re realized within thirty minutes. [illegible]whil[illegible]moval rates of the Cr(VI) no photocatalysts o[illegible]t is [illegible]ovious, which indicates that the Cr (VI) remov[illegible]y photocatalyst is feasible. It is commonly believed that p[illegible]has a great effect against the reduction of Cr(VI). The effec[illegible]s for the pH value of the initial solution (between 2.0 and 5.0) against the photocatalytic Cr(VI) reduction in existence of the complexes **1** and **2** are confirmed in Fig. 3d. Significantly, the reduction for the Cr(VI) can be accelerated by the decrease of pH value. Under ultraviolet irradiation, the reduction rate of Cr(VI) can reach 100% in thirty minutes when pH = 2.0. Furthermore, when the pH value raised from 2.0 to 5.0, the reduction rate for the Cr(VI) decreased from 100% to 60.7%. On the basis of the former reports, $Cr_2O_7^{2-}$ is the main form the condition at lower pH value. Significantly, a large number of H^+ enhances the photocatalytic reduction for the Cr(VI) under the conditions of acid. Therefore, when the pH value is low, the removal ratio for the Cr(VI) is high (Fig. 3d). In addition, at the higher pH value, Cr(III) can precipitate into $Cr(OH)_3$, which is attached to the surface of photocatalyst and covers their active centers, resulting in the decrease of Cr(VI) reduction rate.

In order to deep assess the photocatalytic performances of complexes **1** and **2**, four classical organic dyes of RhB, MB, X-3B and MO were chosen as the organic pollutants, and the degradation experiments were carried out under the irradiation of ultraviolet. As revealed in Fig. 4, the adsorption of complex **1** as well as complex **2** on the four organic dyes can be neglected. The result of photocatalytic experiment exhibits that under ultraviolet irradiation, complexes **1** and **2** were used as the photocatalysts to degrade almost 100% Cr(VI) in 18 min. Complexes **1** and **2** also showed excellent photocatalytic properties for RhB, MB, X-3B under the ultraviolet irradiation. Specifically, complex **1** can degrade MB of 95%, RhB of 89% and X-3B of 97% in thirty minutes, while complex **2** can degrade MB of 94%, RhB of 83% and X-3B of 99% in thirty minutes. While without complexes **1** and **2**, only about 30% RhB, 20% MB, 14% X-3B and 13% MO were decomposed under ultraviolet irradiation in thirty minutes. And as the free ligand H_4L as the photocatalyst, about 71% RhB, 32% MB, 27% X-3B and 49% MO were decomposed under same conditions. Compared with P25 as the photocatalyst, 64% RhB, 86% MB, 17% X-3B as well as 13% MO were destroyed. The results suggested that these two novel coordination polymers revealed outstanding photocatalytic

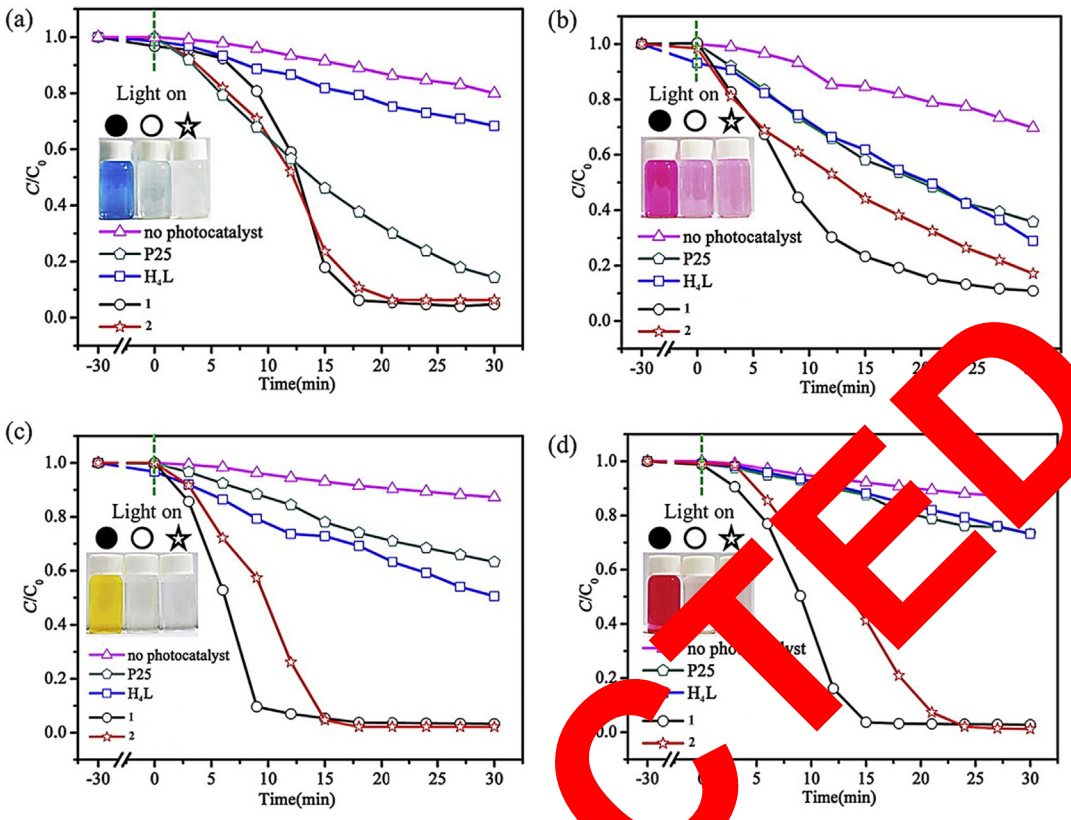

Fig 4 Photocatalytic degradation properties complex **1** [illegible] complex **2** [illegible] solution of MB (a) and RhB (b), MO (c) as well as X-3B (d).

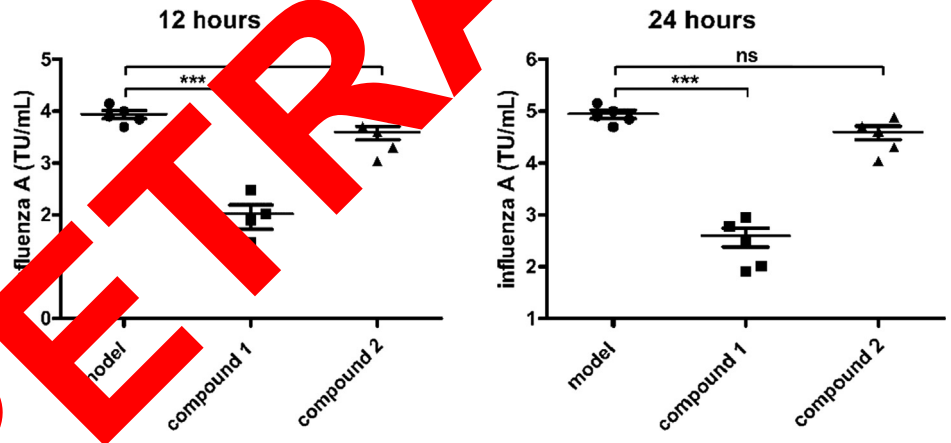

Fig. [illegible] of the influenza A virus into macrophages after complex treatment. The macrophages were plated into cell culture p[illegible] and infected with influenza A virus, after treated with complex **1** or complex **2**. The viral gene transduction of influenza A was determ[illegible] assess the treatment activity for complexes.

properties on both degradation of the organic pollutants and reduction for the Cr(VI).

4.3. Complex inhibited the invasion of the influenza A virus into macrophages

The invasion ability was the significantly character of the influenza A virus. After invaded into the macrophages, the virus could interfere the anti-virus response in the cells. Thus, in this experiment, the viral gene transduction of influenza A was measured to assess the treatment activity for complex **1** and the complex **2**. According to the results of Fig. 5, in comparison with control model, the influenza A virus invaded into the macrophages were much higher in model group. However, after treated with complex **1**, the invasion ability of the influenza A virus was obviously

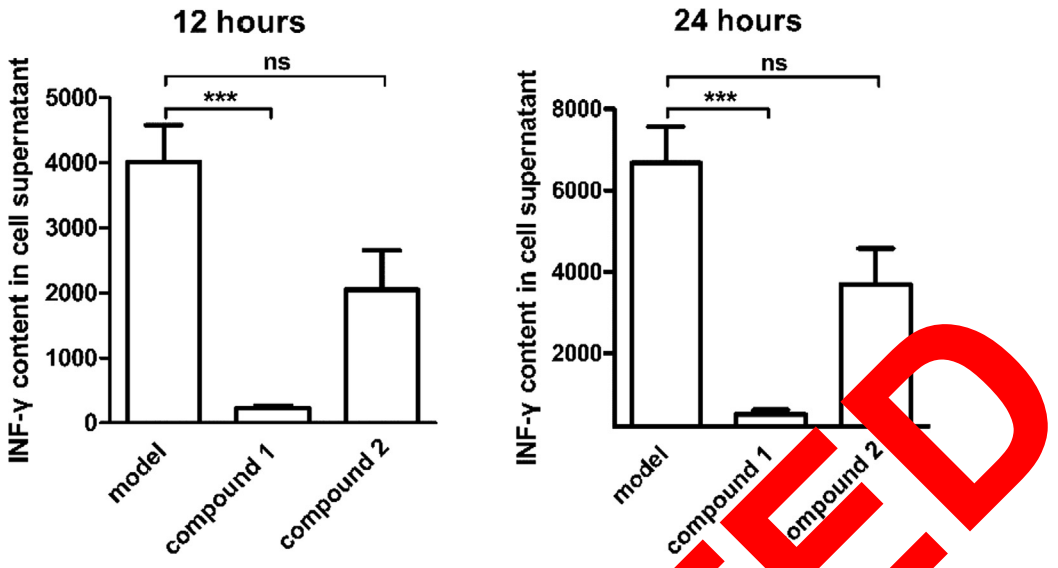

Fig. 6 Increased releasing level of the cytokine INF-γ in macrophages after complex t[illegible]ment. The [illegible]ros[illegible]es were plated into cell culture plates and infected with influenza A virus, followed by complex **1** or **2** treat[illegible] ELISA was us[illegible] detect the INF-γ cytokine released by infected macrophages.

inhibited, but complex **2** possesses nearly no influence against the influenza A invasion ability.

4.4. Complex increased the releasing of the cytokine INF-γ

In the former research, we were demonstrated the exce[illegible]t inhibitory activity for the complex against the influenza invasion ability into macrophages. But how the complex exe[illegible] other protective effects was still needed t[illegible]plored. According to the important role of the cyt[illegible]es in [illegible] infection disease, the ELISA was conducted a[illegible] INF[illegible]ed from macrophages was measured at [illegible]lf a[illegible]d one [illegible]

aft[illegible]he infection. The results in Fig. 6 suggested that compa[illegible]d with the [illegible]ificantly reduced the INF-γ level in model gr[illegible] complex [illegible] treatment could obviously increase the INF[illegible]roduct[illegible] in infected macrophages. While, complex **2** revea[illegible]y without influence against the INF-γ production in infected macrophages.

4.5. Complex induced the expression of the ifitm gene in infected macrophages

The interferon inducible transmembrane proteins (IFITM) is known as an anti-virus protein, which could disturb the

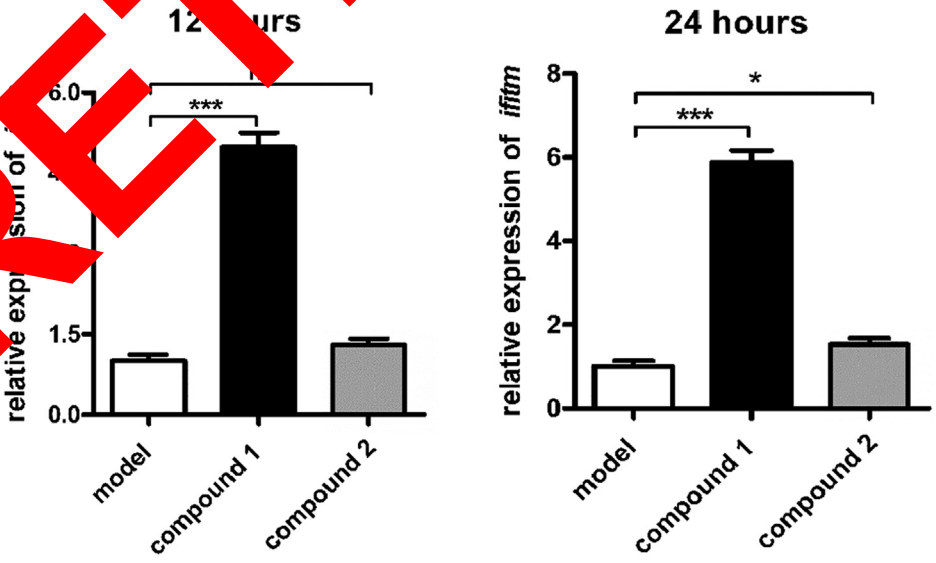

Fig. 7 Induced *ifitm* gene expression level in infected macrophages after treated with complex. The macrophages were plated into cell culture plates and infected with influenza A virus, after treated with complex **1** or **2**. The *ifitm* gene expression level in infected macrophages was detected via the RT-PCR.

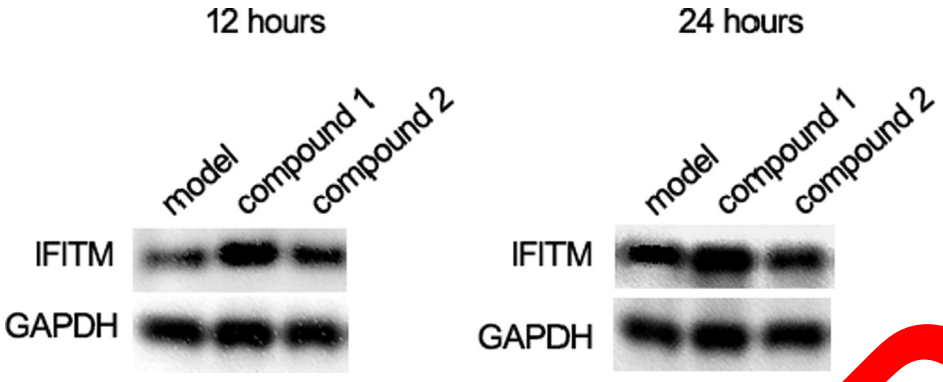

Fig. 8 Down-regulated expression of the IFITM on infected macrophages after complex treatment. The macrophages were plated into cell culture plates and infected with influenza A virus, after treated with complex **1** or **2**. The IFITM expression on infected macrophages was detected by western blot at indicated time.

invasion ability of the virus into macrophages. Thus, after treated with complex **1** or **2**, the *ifitm* gene relative expression levels in infected macrophages was also assessed by the real time RT-PCR. The results in Fig. 7 revealed that in comparison with control group, the *ifitm* gene expression level was much lower in model group. Different from the model group, complex **1** treatment could obviously enhance the *ifitm* gene expression level in infected macrophages. The complex **2** still possesses no influence against the expression of *ifitm* gene.

4.6. Complex down-regulated the expression of the IFITM on infected macrophages

In addition to the previous RT-PCR test, the western blot method was also conducted to assess the IFITM expression on infected macrophages. In the Fig. 8, we can see the expression level of the IFITM on infected macrophages was much lower that of control group, which is consistent with RT-PCR results, suggesting the anti-virus ability of infected macrophages was damaged. While, after treatment with complex **1**, the IFITM expression level was obviously enhanced, while less stronger complex **2**. This result revealed that in comparison with complex **2,** complex **1** possesses stronger treatment activity on influenza A virus infection.

Fig. 8 Down-regulated expression of the IFITM on infected macrophages after complex treatment. The macrophages were plated into cell culture plates and infected with influenza A virus, after treated with complex **1** or **2**. The IFITM expression on infected macrophages was detected by western blot at indicated time.

5. Conclusion

Inconclusion, two fresh coordination polymers based on Cu have been synthesized and then characterized through the analysis of single-crystal X-ray diffraction. The photocatalytic reduction for the Cr(VI) and dye degradation were performed with these two CPs. The results showed that under the ultraviolet irradiation, they revealed excellent photocatalytic reduction for the Cr(VI) in thirty minutes, and the efficiency of reduction was over 98%. From biological result, we can see complex **1** has stronger treatment activity on influenza A virus infection than complex **2**. Then, the ELISA test exhibited that complex could significantly regulated the releasing the INF-γ, but not complex **2**. Next, the results of RT-PCR suggested that complex **1** was better than complex **2** on reducing the relative expression of interferon inducible transmembrane proteins (IFITM). Finally, the western blot further confirmed the induced ability of complex **1** on the IFITM in protein level. In summary, the complex possesses stronger treatment activity than complex **2** on influenza A virus infection through inducing the IFITM expression on macrophages.

Data availability

The data to support the findings of this study are included within the article.

Declaration of Competing Interest

The authors declare that they have no known competing financial interests or personal relationships that could have appeared to influence the work reported in this paper.

Acknowledgments

This study was founded by Beijing JST research (ZR-201921).

Appendix A. Supplementary material

Supplementary data to this article can be found online at https://doi.org/10.1016/j.arabjc.2020.06.021.

References

Bailey, H.E., 2020. Acute necrotizing encephalopathy associated with influenza A. Neuro. J. 60, 41–49.

Bravo-Gómez, M.E., García-Ramos, J.C., Gracia-Mora, I., Ruiz-Azuara, L., 2009. Antiproliferative activity and QSAR study of copper(II) mixed chelate [Cu(N-N)(acetylacetonato)]NO_3 and [Cu(N-N)(glycinato)]NO_3 complexes, (Casiopeínas). J. Inorg. Biochem. 103, 299–309.

Chao, T.L., Gu, S.Y., Lin, P.H., Chou, Y.T., Ling, T.Y., Chang, S.Y., 2020. Characterization of influenza A virus infection in mouse pulmonary stem/progenitor cells. Front. Microbiol. 10, 2942.

Chen, C., Yin, S., Wei, Z., Qiu, Q., Zhu, N., Fan, Y., Pan, M., Su, C., 2019. Pressure-induced multiphoton excited fluorochromic metal-organic frameworks for improving MPEF properties. Angew. Chemie Int. Ed. 58, 14379–14385.

Chen, D.M., Zhang, X.J., 2019. Stepwise and hysteretic sorption of CO_2 in polycatenated metal-organic frameworks. CrystEngComm 23, 4696–4700.

Cui, L., Meng, X., Li, Y., Huang, K., Li, Y., Long, J., Yao, P., 2019. Syntheses, structural diversity, and photocatalytic-degradation properties for methylene blue of Co(II) and Ni(II) MOFs based on terephthalic acid and different imidazole bridging ligands. CrystEngComm 21, 3798–3809.

Duan, C., Yu, Y., Yang, P., Zhang, X., Li, F., Li, L., Xi, H., 2020a. Engineering new defects in MIL-100(Fe) via a mixed-ligand approach to effect enhanced volatile organic compound adsorption capacity. Ind. Eng. Chem. Res. 59, 774–782.

Duan, C., Yu, Y., Xiao, J., Zhang, X., Li, L., Yang, P., Wu, J., Xi, H., 2020b. Water-based routes for synthesis of metal-organic frameworks: a review. Sci. China Mater. 63, 667–685.

Feng, X., Ling, X.L., Liu, L., Wang, L.Y., Ng, S.W., Su, B.Y., 2013. A series of 3D lanthanide frameworks constructed from aromatic multi-carboxylate ligand: structural diversity, luminescence and magnetic properties. Dalton T. 42, 10292–10303.

Feng, X., Feng, Y.Q., Guo, N., Sun, Y.L., Zhang, T., Ma, L.F., Wang, L.Y., 2017. Series d−f heteronuclear metal−organic frameworks: color tunability and luminescent probe with switchable properties. Inorg. Chem. 56, 1713–1721.

Li, Y., Zhang, R., Zhou, W., Wu, X., Zhang, H., Zhang, J., 2019. Hierarchical MoS_2 hollow architectures with abundant Mo vacancies for efficient sodium storage. ACS Nano 13, 5533–5540.

Mifsud, E.J., Tilmanis, D., Oh, D.Y., Ming-Kay, T.C., Rossignol, J. F., Hurt, A.C., 2020. Prophylaxis of ferrets with nitazoxanide and oseltamivir combinations is more effective at reducing the impact of influenza a virus infection compared to oseltamivir monotherapy. Antiviral Res. 176, 104751.

Mukhopadhyay, P., Iwashita, Y., Shirakawa, M., Kawano, S., Fu[illegible] N., Shinkai, S., 2006. Spontaneous colorimetric sensing [illegible] positional isomers of dihydroxynaphthalene in a 1D organogel matrix. Angew. Chem. Int. Edit. 45, 1592–1595.

Pan, M., Liao, W.M., Yin, S., Sun, S.S., Su, C., 2018. Single-phase white-light-emitting and photoluminescent color-tuning coordination assemblies. Chem. Rev. 118, 8889–8935.

Rivero-Müller, A., De Vizcaya-Ruiz, A., Plant, N., Ruiz, L., Dobrota, M., 2007. Mixed chelate copper complex, Casiopeina iigly, binds and degrades nucleic acids: a mechanism of cytotoxicity. Chem. Biol. Interact. 165, 189–199.

Ruiz-Azuara, L., Bravo-Gomez, M.E., 2010. Copper compounds in cancer chemotherapy. Curr. Med. Chem. 17, 3606–3615.

Stewart, W.W., 1981. Lucifer dyes—highly fluorescent dyes for biological tracing. Nature 292, 17–21.

Tang, J., Salunkhe, R.R., Zhang, H., M[illegible]as, [illegible]hamad, T., Alshehri, S.M., Kobayashi, N., Tom[illegible]a, S., Ide, [illegible]Kim, J.H., Yamauchi, Y., 2016. Bimetallic m[illegible]organic fra[illegible]orks for controlled catalytic graphitiza[illegible]n of [illegible]porous c[illegible]ons. Sci. Rep. 6, 30295.

Xu, G., Zhang, H., Wei, J[illegible]iang, [illegible]X., Wu[illegible], Y., Li, C., Zhang, J., Ye, J., 2018[illegible]yratin[illegible]g-C3N4 n[illegible]osheet with B-H bonding decorated meta[illegible]framew[illegible]for CO_2 activation and photoreduct[illegible]ACS [illegible]12, 533[illegible]540.

Yanagi, H., Oz[illegible]H., 2019. [illegible]syndrome complicating influenza A[illegible]fection. J. Ge[illegible]m. Med. 21, 18–20.

Zhang, H., W[illegible]g, T., [illegible]g, J., Liu, H., Dao, T.D., Li, M., Liu, G., Meng, Y., Chang, K[illegible] L., Nagao, T., Ye, J., 2016. Surface-p[illegible]nhanced photo[illegible]n CO_2 reduction catalyzed by metal–[illegible]anic-framework-derived iron nanoparticles encapsulated by [illegible]rathin carb[illegible]ayers. Adv. Mater. 28, 3703–3710.

Zh[illegible]H., Zhou, [illegible], Dong, J., Lu, X.F., (David) Lou, X.W., 2019. [illegible]molecula[illegible]ectronic coupling in porous iron cobalt (oxy) ph[illegible]oboxes enhances the electrocatalytic activity for oxygen evolution. Energy Environ. Sci. 12, 3348–3355.